Peer-reviewed version available at *Materials* **2018**, *11*, 2341; doi:10.3390/ma11112341

Article

Comparison of cohesive models in EDEM and LIGGGHTS for simulating powder compaction

Cristina Ramírez-Aragón[1], Joaquín Ordieres-Meré [2,*], Fernando Alba-Elías [1] and Ana González-Marcos [1]

[1] Department of Mechanical Engineering, University of La Rioja, C/ Luis de Ulloa, 20, 26004, Logroño, La Rioja, Spain; maria-cristina.ramirez@alum.unirioja.es; fernando.alba@unirioja.es; ana.gonzalez@unirioja.es
[2] Department of Industrial Engineering, Business Administration and Statistics, Polythecnic University of Madrid, C/ José Gutiérrez Abascal, 2, 28006, Madrid, Spain; j.ordieres@upm.es
* Correspondence: j.ordieres@upm.es; Tel.: +34 91 336 31 44

Abstract: The purpose of this work was analysing the compaction of a cohesive material using different DEM simulators to determine the equivalent contact models and identify how some parameters of the simulations affect the compaction results (maximum force and compacts appearance) and computational costs. For that purpose, three cohesion contact models were tested ('linear cohesion' in EDEM; 'SJKR' and 'SJKR2' in LIGGGHTS). The influence of the particle size distribution (PSD) on the results was also investigated. Further assessments were performed on the effect of selecting different timesteps, using distinct conversion tolerances for exporting the 3D models to STL files and moving the punch with different speeds. Consequently, it was possible to determine that a timestep equal to a 10% Rayleigh timestep, a conversion tolerance of 0.01 mm and a punch speed of 0.2 m/s are adequate for simulating the compaction process using the contact models in this work. In addition, the results determined that the maximum force was influenced by the PSD because of the rearrangement of the particles. The PSD was also related to the computational cost because of the number of simulated particles and their sizes. Finally, an equivalence was found between the linear cohesion and SJKR2 contact models.

Keywords: Powder compaction; Discrete element method (DEM); Cohesive contact models; LIGGGHTS; EDEM

1. Introduction

Sintering is a processing technique of consolidation of powders by applying thermal energy. This technique allows to produce density-controlled parts from metal or ceramic powders as well as combination of them to obtain composites. Typically, three processing steps involve the fabrication of sintered parts: preparation of a powder blend, compaction of the powder to form a green compact and consolidation of the green compact at high temperatures [1]. The techniques used in each of these steps and the variables involving them may influence the properties of the sintered parts [2–4]. Although all of the processing steps affect the sintered parts, the compaction is crucial because the powder sintering ability is closely related to the packing density [5]. For example, the sizes of the powder particles influences the pore sizes of the sintered parts because the pores are formed from the interstices of the powder particles [6]. The shape of the particles also has an effect on the packing density and the sintering behaviour [7]. For that reason, it is important to know how some factors affect the compaction of the powders because a better understanding of this process will allow to improve the green compacts and, therefore the sintered parts.

The discrete element method (DEM) has been used to examine the behaviour of different materials during the formation of a compact. Janda and Ooi [8] simulated the consolidation process of real soils by modelling a uniaxial confined compression. Then, they used the same model for analysing the penetration resistance of cohesive soils. Thakur et al. [9] simulated the compaction of detergent powders to form a cylindrical sample and analysed the relationship between the porosity

of the compact and consolidation stress. The results were contrasted with experimental data. Following this, an unconfined compression test was simulated. The stress-strain curves during the failure were also compared. Aranda [10] simulated the compaction of a refractory disc using different particle size distributions (PSDs) and materials. The porosity and permeability of the compacts were analysed in all the cases. Other authors studied the effect of the PSD [11,12] and examined the influence of the particle shape [13,14] on compaction process.

Different software packages for DEM simulating have been appearing in recent years. Some of them, such as EDEM, ROCKY and PFC, are commercially distributed, but other ones, like LIGGGHTS or YADE, are open-source packages. Moreover, all these software programs provide several contact models, so it is possible to choose the most appropriate for simulating different processes or systems. For example, Jiménez-Herrera et al. [15] simulated the breakage of particle beds due to the impact of a ball using three contact models. Two of them were implemented in EDEM and the other one in ROCKY. Some features, including the facility of using each model and the similitude of the simulation results with an experiment, were analysed. Another interesting approach is comparing the results using different simulation packages; for example, Wei et al. [16] investigated the charging system of an ironmaking blast furnace using EDEM and LIGGGHTS. The results obtained using each software program were compared. Moreover, a good agreement was found between them and the experimental data. Similarly, Markauskas et al. [17] compared the results obtained using EDEM and DEMMat during a silo discharge. Soltanbeigi et al. [18] used the multisphere approach in EDEM and superquadric shapes in LIGGGHTS for simulating the behaviour of nonspherical particles during different processes, such as heap formation, shear testing or discharging of a silo. They also compared the results obtained using both software programs. Kozhar et al. [19] tested an irregular shaped particle under uniaxial compression and then simulated it with DEM. They used two software for that purpose: EDEM and MUSEN. Two contact models were applied in EDEM, where a multi-sphere approach was used to simulate the irregular shape of the particle. In MUSEN, the particle was simulated with a bonded-particle model, where different models defined the characteristics of the bonds.

To satisfy the recent interest that the existence of different DEM simulators and contact models has generated, in this work, DEM was used to analyse the capability of some cohesion contact models to simulate the compaction of a granular mixture to form a compact. A system that consists of a matrix and two punches was used for this purpose. Three cohesion contact models implemented in two software packages were applied to simulate the particles' behaviour. The results obtained using the different contact models were compared to determine which are equivalent. Specifically, the analysis considered the maximum force applied by the upper punch, percentage of eliminated contacts after the ejection of the compact and computational costs that the simulations require. Three PSDs were modelled to observe the influence of the materials' granulometric properties on the compaction process. Moreover, the influence of some parameters, such as the timestep, geometries or speed of the punch on the results, was studied. Thus, the optimal values of these parameters for simulating the compaction process using these contact models were determined. Consequently, these values could be utilised in future works to model the compaction of other materials.

Although the effects of the PSD or the speed of the punches on the compaction process is widely known, the novelty of this work is the use of different DEM simulators in order to compare several contact models and find equivalent models implemented in each DEM package. Additionally, this manuscript details some of the differences between both simulators during the creation of the DEM model and the actions that were taken to reduce that differences. Thereby, this study can be useful for people that use the commercial package EDEM, but also for people that use the open-source package LIGGGHTS. Moreover, this research can be interesting for researchers that simulate the compaction process because it gives some keys to define the DEM models and reduce the computational cost of the simulations.

2. Materials and Methods

This section presents the characteristics of the DEM models that were simulated using EDEM and LIGGGHTS. It describes how the models were defined in each DEM software in order to prevent differences between both simulators and the details about the methodology that was conducted in this work.

2.1. The discrete element method (DEM)

The discrete element method that Cundall and Strack proposed [20] is a numerical method that is capable of simulating the mechanical behaviour of a granular medium that is composed of an assembly of particles which displace independently and interact with the other ones at their contact points. This method is based on the application of the Newton's second law to the particles and a force-displacement law at the contacts. The properties of the particles (position, velocity, forces acting on them, etc.) are updated at every timestep. Each timestep, a calculation cycle is completed. This cycle begins with the detection of contacts between particles. At this time, the contact point and the overlap between two particles in contact are calculated. Then, they are used to obtain the contact forces by applying the force-displacement laws. Once the forces and the moments applied to each particle have been calculated, the motion of each particles is calculated by the Newton's second law. Thereby, the acceleration, velocity and position of the particles are updated using a time integration algorithm and the calculation cycle is completed. The updated values are used to detect the subsequent contacts and another cycle begins. Because of the updating is carried out by using an explicit integration technique, the timestep must be very small to obtain stable numerical solutions. The maximum value of timestep at which the solutions of the simulations are stable is known as critical timestep. Different criteria to calculate the critical timestep have been defined, but the Rayleigh critical timestep is the most usually utilized. This criteria is calculated as a function of the radius (R), the density (ρ), the shear modulus (G) and the Poisson ratio (υ) of the particles:

$$\Delta T_{Rayleigh} = \frac{\pi R}{0.163\upsilon + 0.8766}\sqrt{\frac{\rho}{G}} \quad (1)$$

The displacements of each particle are obtained by explicitly integrating the Newton's differential equations of motion:

$$m_i \frac{d^2}{dt^2} x_i = \sum_j (F_{n,ij} + F_{t,ij}) + m_i g \quad (2)$$

$$I_i \frac{d\omega_i}{dt} = \sum_j (T_{ij}) \quad (3)$$

Where m_i, I_i, x_i and ω_i are the mass, the moment of inertia, the position and the angular velocity of the particle i, respectively. $F_{n,ij}$, $F_{t,ij}$ and T_{ij} are the normal force, the tangential force and the torque between particles i and j. The effect of rolling friction was ignored in this work, so its calculus is not shown in this section.

The force-displacement laws, named contact models, are used to calculate that forces between particles ($F_{n,ij}$ and $F_{t,ij}$). In this work, a modification of the Hertz-Mindlin (HM) contact model has been used. It consists in the addition of a normal cohesion force ($F_{n,cohesion,ij}$). Therefore, $F_{n,ij}$ and $F_{t,ij}$ are calculated as follows:

$$F_{n,ij} = F_{n,HM,ij} + F_{n,cohesion,ij} \quad (4)$$

$$F_{t,ij} = F_{t,HM,ij} \quad (5)$$

In the Hertz-Mindlin model [21] the normal force is based on the Hertzian contact theory, the theory of Mindlin and Deresiewicz is used to calculate the tangential force and the tangential friction force is calculated according to the Coulomb law of friction. In addition to these forces, a damping component is implemented. The following equations include all of these components.

$$F_{n,HM,ij} = \frac{4}{3} E_{ij} \delta_{n,ij}^{\frac{3}{2}} \sqrt{R_{ij}} - \sqrt{\frac{20}{3}} \frac{(ln\, e)}{\sqrt{ln^2\, e+\pi^2}} \left(m_{ij} E_{ij} \sqrt{R_{ij} \delta_{n,ij}}\right)^{\frac{1}{2}} v_{n,ij} \quad (6)$$

$$F_{t,HM,ij} = min\left[\mu_{s,ij} F_{n,HM,ij}\,, \left| -8 G_{ij} \delta_{t,ij} \sqrt{R_{ij} \delta_{n,ij}} - \sqrt{\frac{80}{3}} \frac{(ln\, e)}{\sqrt{ln^2\, e+\pi^2}} \left(m_{ij} G_{ij} \sqrt{R_{ij} \delta_{n,ij}}\right)^{\frac{1}{2}} v_{t,ij} \right| \right] \quad (7)$$

Where $\delta_{n,ij}$, $\delta_{t,ij}$ are the normal and tangential overlap between particles i and j, respectively. $v_{n,ij}$ and $v_{t,ij}$ are the normal and tangential components of the relative velocity between particles i and j, respectively. $\mu_{s,ij}$ is the coefficient of static friction between particle i and j. E_{ij} is the equivalent Young's modulus, G_{ij} is the equivalent shear modulus, R_{ij} is the equivalent radius and m_{ij} is the equivalent mass. They are defined as:

$$\frac{1}{E_{ij}} = \frac{1-\nu_i^2}{E_i} + \frac{1-\nu_j^2}{E_j} \quad (8)$$

$$\frac{1}{G_{ij}} = \frac{2-\nu_i}{G_i} + \frac{2-\nu_j}{G_j} \quad (9)$$

$$\frac{1}{R_{ij}} = \frac{1}{R_i} + \frac{1}{R_j} \quad (10)$$

$$\frac{1}{m_{ij}} = \frac{1}{m_i} + \frac{1}{m_j} \quad (11)$$

The normal cohesion force is calculated as follows:

$$F_{n,cohesion,ij} = k_{ij} A_{ij} \quad (12)$$

Where k_{ij} is the cohesion energy density and A_{ij} is the contact area between particles i and j.

2.2. DEM simulations

The DEM simulations were performed using two different software programs, as follows: EDEM® 2.7.2 (DEM Solutions Ltd., Edinburgh, Scotland, UK) and LIGGGHTS® version LIGGGHTS-PUBLIC 3.3.1. EDEM is a commercial software program that uses an intuitive graphical user interface consisting of three simulation components. These components allow completion of all the processes that simulations involve (preprocessing, simulation and postprocessing) using unique DEM software. The creator component is employed to define the properties of the materials of particles and geometries, contact models and so on (preprocessing). The configuration and control of the simulation process are performed by the simulator component. Finally, the analyst component allows the results to be visualised, analysed and exported (postprocessing). LIGGGHTS is open-source software that uses a command line interface to complete the preprocessing and simulation processes. However, the results that this package provides require other tools for analysis and visualisation. Consequently, the postprocessing of the simulations that were run in LIGGGHTS was performed using PARAVIEW version 4.4.0 64-bit. The simulations were conducted on a server with 64 GB of

RAM with a 2 x Intel Xeon Quad-core 2.0 GHz E5504 CPU. The simulations in LIGGGHTS were run on a single processor. In contrast, the simulations in EDEM were run in batch mode using four cores.

To search for equivalent cohesion contact models in both DEM packages, three contact models were used in this work. The 'linear cohesion' contact model was used in the simulations run in EDEM. In LIGGGHTS, the simplified Johnson–Kendall–Roberts ('SJKR') and modified SJKR ('SJKR2') models were applied. The reason for choosing these contact models is that they all calculate the cohesion force as a normal force that is proportional to the contact area, as shown in Equation 12. Other cohesion contact models are available in both software programs, but they consider other forces, such as the liquid bridge force (e.g. the 'Hertz–Mindlin with JKR cohesion' model in EDEM or 'easo/capillary/viscous' and 'washino/capillary/viscous' models in LIGGGHTS). This means that other parameters (different from the cohesion energy density and contact area) were considered for the calculus of the force. Therefore, the equations that define the cohesion force are also different. However, although the three contact models that were used in this work seem to be equivalent, they calculate the contact area in different ways. The contact area in the SJKR2 and linear cohesion models is calculated as a simplification of the contact area used in the SJKR model. The contact area (A_{ij}) between particles i and j, is calculated in each contact model as follow:

$$A_{ij(SJKR)} = \frac{\pi}{4}\frac{(-d+R_i+R_j)(d+R_i-R_j)(d-R_i+R_j)(d+R_i+R_j)}{d^2} \quad (13)$$

$$A_{ij(SJKR2,linear\ cohesion)} = 2\pi\delta_{n,ij}R_{ij} \quad (14)$$

Where R_i and R_j are the radius of the particles i and j, respectively, d is the distance between their centres, $\delta_{n,ij}$ is the normal overlap between particles i and j, that is calculated as R_i+R_j-d and R_{ij} is the equivalent radius (see Equation 10).

Despite this difference, it could be interesting to analyse how the results and computational costs are influenced by this factor. The effect of the rolling friction was ignored in all cases. The coefficient of static friction was 0.5 and the coefficient of restitution was 0.2 for all the possible interactions (particle–particle, particle–wall and wall–wall). Moreover, the cohesion effect was applied only to the interparticle contacts. The value of cohesion energy density was 3×10^6 J/m^3 in all the simulations.

The compaction mechanism in the uniaxial presses used to form green compacts is generally composed of two punches and a matrix. The punches compact the powder into the required shape that is determined by the shape of the matrix when pressure is applied. The geometries of the components that were used in this work and their dimensions can be seen in Figure 1. The process that was simulated in this work consists of the three following stages, as shown in Figure 2: the creation of the particles, compaction process and compact ejection. During the creation process, the particles are created in a cylindrical factory. This factory is a virtual geometry located in the initial assembly of the physical components (punches and matrix). At this moment, the upper punch is located at a distance of 25 mm from the lower punch. After the particle creation is completed, the compaction process begins by moving down the upper punch with a constant velocity. This movement stops when the distance between the punches is equal to 8 mm. At this moment, the upper punch applies the maximum force. Then, the upper punch begins its upward movement with the same velocity. The movement ceases when the upper punch is placed at a height of 16 mm. Finally, the matrix is removed, and the simulation process ends after waiting for 0.05 seconds. To simulate this process, the geometries of each component (punches and matrix) were generated on computer-aided design (CAD) software and then imported into the DEM software as STL files.

Peer-reviewed version available at Materials 2018, 11, 2341; doi:10.3390/ma11112341

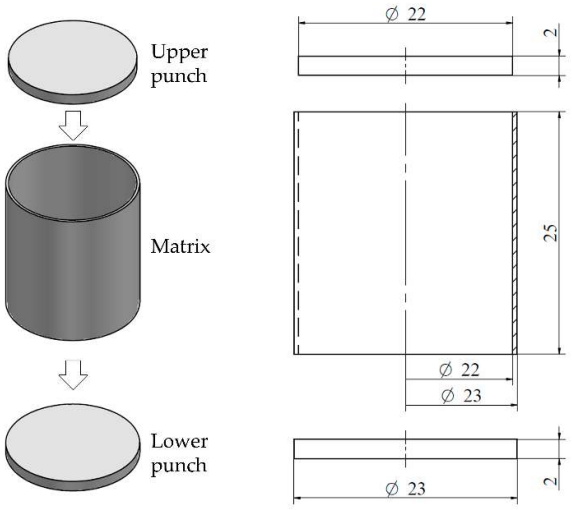

Figure 1. Geometries used in DEM simulations.

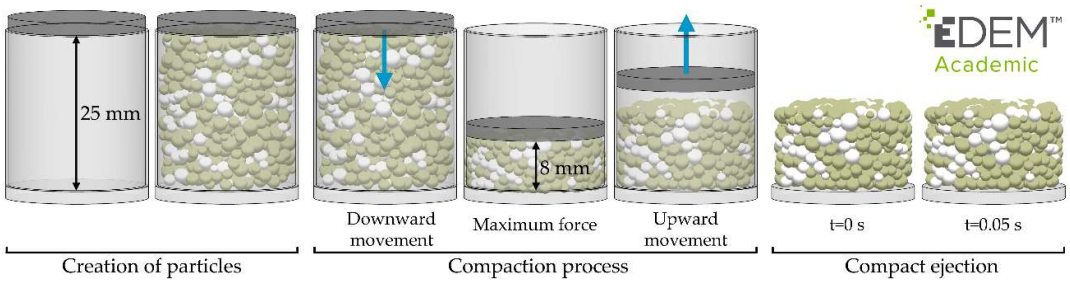

Figure 2. Stages in the simulated process.

Two granular materials were simulated in this work. Their properties are shown in Table 1. Although the particle sizes of these materials are unreal, their properties are similar to those of some refractory materials. Moreover, a combination of different refractory materials is commonly used in the metallurgical industry [22]. Thus, a mixture of materials 1 and 2 in weighted proportions of 80% and 20%, respectively, was used. To examine the influence of the size particle, three different PSDs of these materials were analysed. These PSDs were as follows: monosized particles (MP), uniform distribution (UD) and normal distribution (ND). The sizes of all the particles were the same in the first PSD (MP). The mixture of the second one (UD) consisted of the same proportions (by weight) of each particle size. The sizes of the particles followed a normal distribution in the last one (ND). Figure 3 shows the number of particles of each size that were created to simulate the mixtures using the different PSDs.

Table 1. Summary of material properties used in DEM simulations.

Material properties			
	Material 1	**Material 2**	**Wall**
Mean diameter (mm)	2.1	2.1	-
Density (kg/m3)	3500	3000	8000
Young's modulus (Pa)	2.5×10^8	2.5×10^8	2.0×10^8
Poisson's ratio	0.25	0.25	0.25

Preprints (www.preprints.org) | NOT PEER-REVIEWED | Posted: 4 October 2018 doi:10.20944/preprints201810.0081.v1

Peer-reviewed version available at Materials 2018, 11, 2341; doi:10.3390/ma11112341

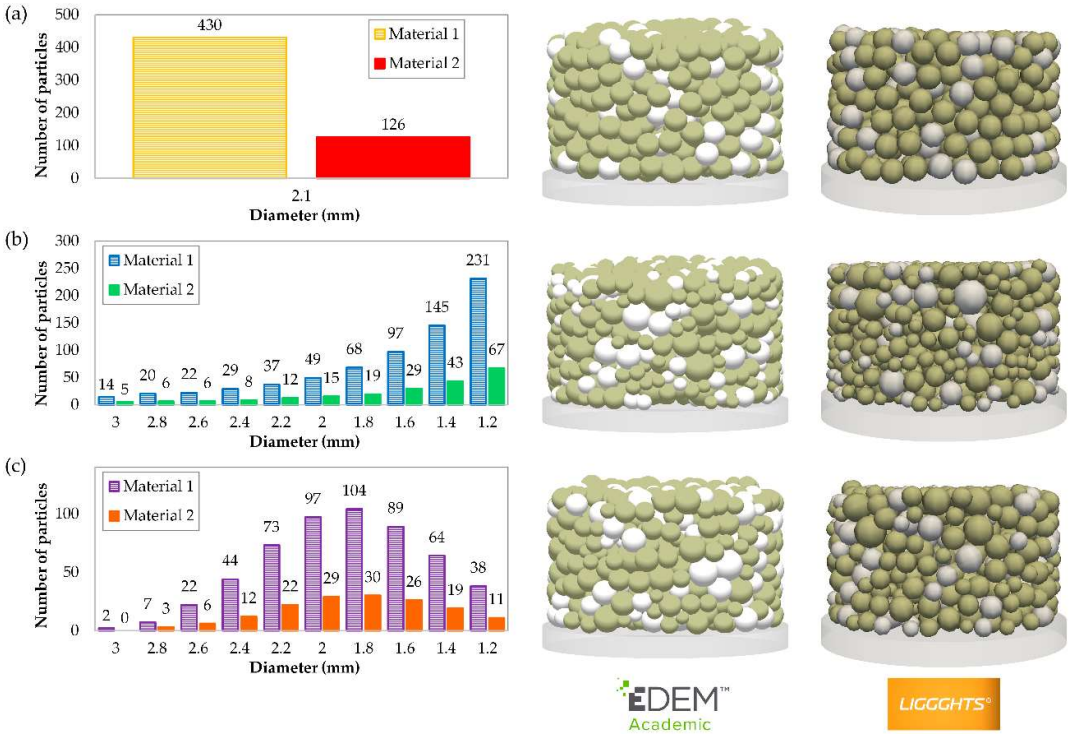

Figure 3. Number of particles used in discrete element method (DEM) simulations and appearance of compacts obtained in both software programs with different particle size distributions (PSDs): (a) monosized particles (MP), (b) uniform distribution (UD) and (c) normal distribution (ND).

The simulations were initially run in LIGGGHTS. After the visualisation of the simulated system in PARAVIEW, the simulations were conducted in EDEM. Thus, the simulations in EDEM were modelled exactly like their homologues in LIGGGHTS. This was possible because of the control of all the parameters and dynamics of the models throughout the EDEM interface. Some of the considerations that were taken up are explained below.

Both software programs enabled automatic creation of a set of particles with different PSDs (uniform distribution, Gaussian distribution, etc.). However, the number of particles of each size could vary in the different simulations using these options. Thus, none of the automatic options was used in EDEM to create the particles; instead, the number of particles of each size was introduced manually. As a result, the same number of particles of each size was used in both programs.

Another difference in the creation of the particles was evaluated. Most of the types of particle insertion in LIGGGHTS use the flag 'all_in', which enables particle insertion into the factory (virtual geometry) in two ways. The value of this flag determines whether the particles are completely contained in the factory (when the value of the flag is 'yes') or only their centres (when the value is 'no'). This is important when one wants to insert particles into a physical geometry, as the factory dimensions must be adapted depending on the case. If the particles are completely contained in the factory (all_in = yes), the factory surfaces can coincide with the physical ones. However, the factory must be reduced if only the centres of the particles are located in the factory (all_in = no) because the particles can be created in the surface of the physical geometry. The particles that are partially introduced in the physical surfaces are caught in the geometries or exit them. Nevertheless, this option does not exist in EDEM. The centres of the particles can be created in the virtual surfaces of the factory when this is not in contact with a physical geometry; however, the particles are all located in the factory when its virtual surfaces coincide with the surfaces of the physical geometries. EDEM automatically detects the surfaces of the physical geometries and prevents the creation of the particles in these surfaces. Figure 4 shows how the particles are created in reduced and unreduced factories in both software programs and sets the flag 'all_in' with the values 'yes' and 'no' in LIGGGHTS. To

generate equivalent simulation models, the factories used in both programs coincided with the inner surfaces of the physical geometries, and the value 'yes' was assigned to flag 'all_in' in LIGGGHTS.

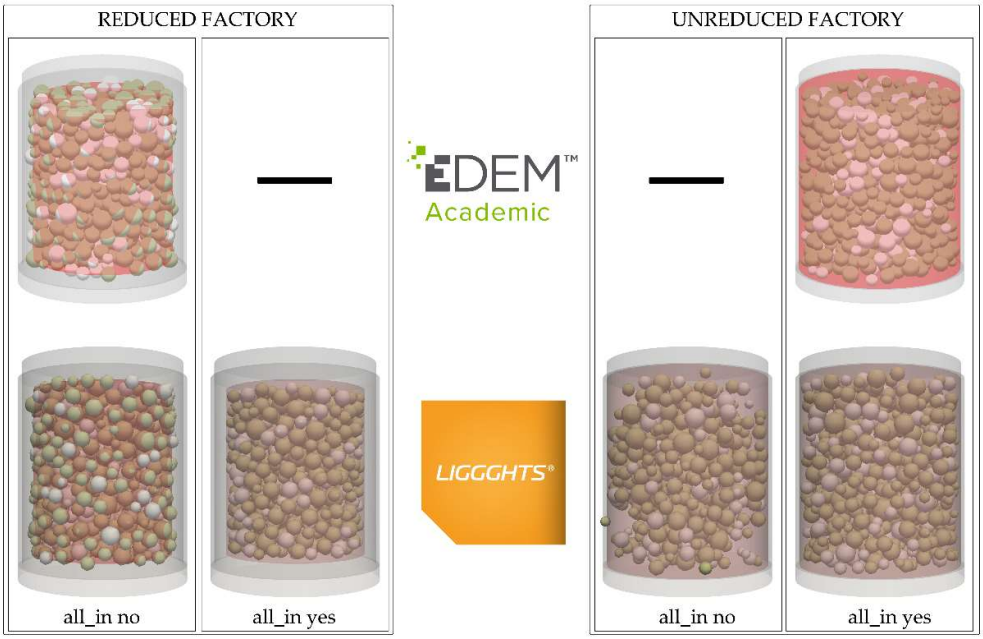

Figure 4. Insertion of particles. Equivalences between EDEM and LIGGGHTS.

2.3. Methodology

This work analysed the relationship between five parameters introduced in simulations (timestep, conversion tolerance, speed of the upper punch, PSD and contact model) and three critical factors that determine the goodness of the simulations and their efficiency, namely the maximum force that is applied by the upper punch, percentage of eliminated contacts (related to the final appearance of the compact) and computational cost. First, the influence of the timestep was examined. For this purpose, six simulations (Table 2, setup no. 1–6) using different timesteps were conducted for all the PSDs and contact models. The timestep values were approximately equivalent to the values of 5, 10, 15, 20, 25 and 30% Rayleigh timestep. However, the Rayleigh timestep was higher for the MP distribution than for UD and ND because the latter used smaller particles. Moreover, it was necessary for the timestep values to be divisors of the values of the target save interval (0.001 s in these simulations) to obtain the results at exactly the same times. For these reasons, the values of the timesteps in the simulations of the MP distribution were different from those used in the UD or ND. In addition, the computational cost required to complete these simulations was analysed to obtain the optimal value of the Rayleigh timestep percentage. The use of different geometries was also analysed. For this purpose, the geometries corresponding to the punches and matrix were generated on CAD software and exported as STL files using different conversion tolerances (Table 2, setup no. 2 and 7–9). Thus, the mesh sizes of the geometries became larger as the tolerance increased. Therefore, the geometries with smaller meshes were more similar to the theoretical ones (cylindrical geometries), but they became prisms with a lower number of lateral faces when the sizes of the meshes were greater, as Figure 5 shows. In this work, the effects of using four conversion tolerances on the results and computational cost were analysed to determine the optimum value. Finally, several simulations (Table 2, setup no. 2 and 10–16) were conducted to examine the effect of the punch's speed. The simulation time in the simulations of the compaction process increased proportionally as the speed of the punch decreased, and therefore, the computational cost also increased. For this reason, it was interesting to consider how this parameter influences the results of the simulations and their computational costs to determine the maximum speed that can be applied for obtaining adequate results by employing an acceptable time.

Table 2. Setup of DEM simulations.

Setup number	Timestep (s)		Timestep (% Rayleigh)	Conversion tolerance (mm)	Speed of punch (m/s)
	MP	UD/ND			
1	1.0×10^{-6}	5.0×10^{-7}	~ 5	0.01	0.2
2	2.0×10^{-6}	1.0×10^{-6}	~10	0.01	0.2
3	3.125×10^{-6}	2.0×10^{-6}	~15	0.01	0.2
4	4.0×10^{-6}	2.5×10^{-6}	~20	0.01	0.2
5	5.0×10^{-6}	3.125×10^{-6}	~25	0.01	0.2
6	6.25×10^{-6}	4.0×10^{-6}	~30	0.01	0.2
7	2.0×10^{-6}	1.0×10^{-6}	~10	0.001	0.2
8	2.0×10^{-6}	1.0×10^{-6}	~10	0.1	0.2
9	2.0×10^{-6}	1.0×10^{-6}	~10	1.0	0.2
10	2.0×10^{-6}	1.0×10^{-6}	~10	0.01	0.0005
11	2.0×10^{-6}	1.0×10^{-6}	~10	0.01	0.001
12	2.0×10^{-6}	1.0×10^{-6}	~10	0.01	0.005
13	2.0×10^{-6}	1.0×10^{-6}	~10	0.01	0.01
14	2.0×10^{-6}	1.0×10^{-6}	~10	0.01	0.05
15	2.0×10^{-6}	1.0×10^{-6}	~10	0.01	0.1
16	2.0×10^{-6}	1.0×10^{-6}	~10	0.01	0.5

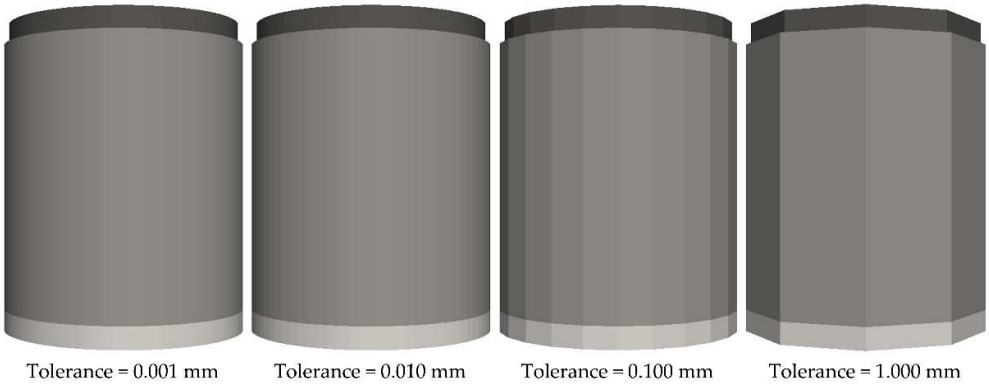

Figure 5. Geometries used to analyse the effect of the conversion tolerance.

The influence of the PSD was analysed by comparing the results of all the simulations. The similarities and differences between the results obtained with the different contact models were also examined through all the simulations.

The three factors mentioned above (maximum force, percentage of eliminated contacts and computational cost) were compared in all the cases. The maximum force applied by the upper punch during the compaction process was analysed. The maximum value of force was attained when the upper punch was located at 8 mm from the lower punch. This factor can be considered most important, as some of the main defects in the compacts are generated by the application of excessive or insufficient force. Consequently, the force is one of the parameters that is usually controlled in experimental testing. In addition, the appearance of the compacts after they were compacted was examined. To quantify this quality of the compacts, the percentage of eliminated contacts (from 0.01 s to 0.05 s after the matrix was removed) was calculated. This parameter is related to the final appearance of the compacts due to a greater percentage of eliminated contacts indicates that the

particles have been separated and the forces that kept them joined have disappeared. If this occurs, the particles could fall and form a heap of particles instead of a compact. Finally, the computational costs of the simulations were compared. Thus, a combined examination of these three factors was performed to determine the optimal values of the timestep, conversion tolerance and punch speed. The optimal values of these parameters will be those that provide adequate results (maximum force and percentage of eliminated contacts) using the minimum computational cost.

3. Results and discussion

The results and discussion are separated into the following five sections. Section 3.1 analyses the effect of the timestep on the maximum force applied by the punch, the percentage of eliminated contacts after the compact ejection and the computational cost. The influence of the conversion tolerance on the results is studied in Section 3.2. Section 3.3 presents the results that were obtained moving the punch at different speeds. The effect of the PSD is discussed in Section 3.4. Finally, Section 3.5 compares the results obtained using the different contact models and established which of the two models implemented in LIGGGHTS is equivalent to the one implemented in EDEM.

3.1. Effect of the timestep

Figure 6 shows the effect of the timestep on the maximum force applied by the punch on the percentage of eliminated contacts after the matrix has been removed and the computational cost of the simulations.

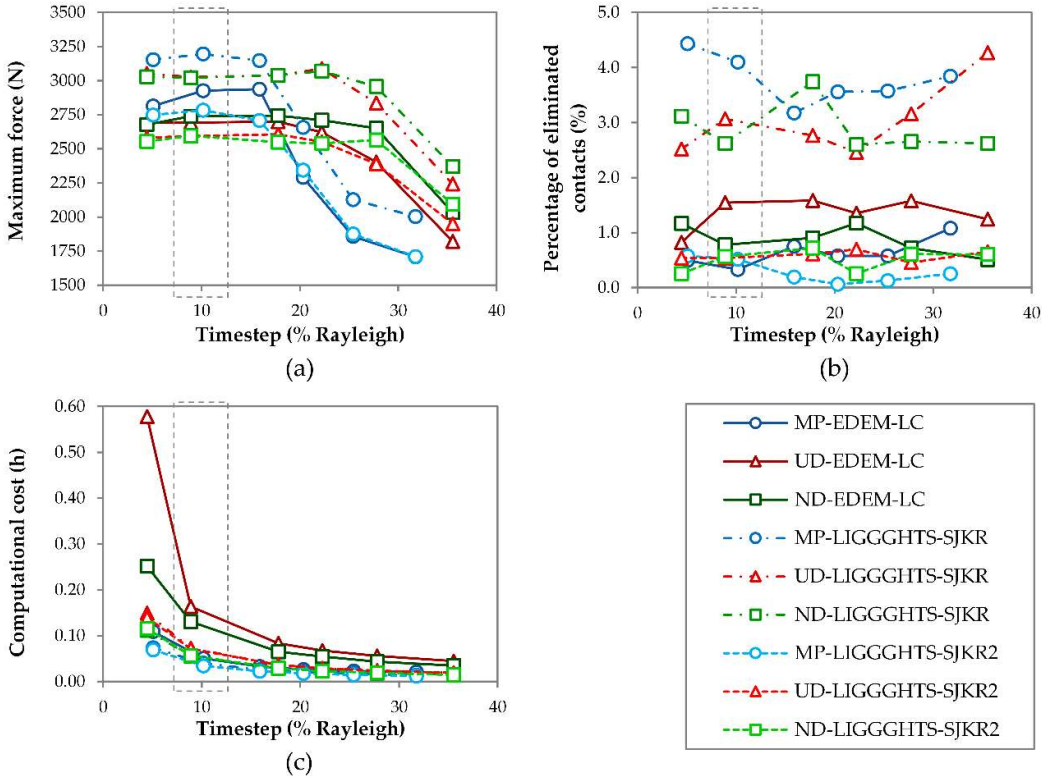

Figure 6. Effect of the timestep on (a) the maximum force applied by the punch, (b) percentage of eliminated contacts after the matrix has been removed and (c) total computational cost.

As evident in Figure 6(a), the maximum force depends on the timestep that is fixed in the simulations. The trend of all the curves is the same. The maximum force remains nearly constant as the timestep increases at low values. However, the force decreases as the timestep increases from a value. This value is approximately equal to 15% of the Rayleigh timestep in the cases of MP and UD, but in the case of ND, the change in the curve is produced near the 25% Rayleigh timestep. This

behaviour is more evident in the case of MP. Moreover, the maximum forces that are applied by the punch in the simulations that used the SJKR model were greater than their homologues using the SJKR2 and linear cohesion models, as Figure 6(a) illustrates. Comparing the calculus of the contact area in each model, one can see that the value of the contact area that is calculated using the Equation 13 (SJKR model) is slightly lower than those calculated using the Equation 14 (SJKR2 and linear cohesion models) for a same pair of particles. Consequently, the cohesion force acting on a pair of particles using the model SJKR is lower than those obtained from the SJKR2 or the linear cohesion models. This makes the updated normal overlap between the pair of particles be lower in the SJKR model than in the other ones if only the cohesion force is acting on the particles. Therefore, the average overlap in an assembly of particles will be also lower for the SJKR model if external forces are not acting on it. As a consequence, the volume that the assembly of particles occupy will be greater for that model. However, the volume that is occupied by the particles when the punch applies the maximum force is the same for all the contact models, i.e. the overlap must be the same in all cases. For that reason, the punch must apply a greater force when the SJKR model is used to achieve the same average overlap that is obtained by using the SJKR2 or the lineal cohesion models. In spite of this difference, the curves obtained in homologue simulations were similar, regardless of the contact model used. The behaviour of all these curves indicates that the simulation models converge at low timesteps, regardless of the PSD and contact model used. This may due to an error in the calculus of the position of the punch or its force when a large timestep is fixed.

Figure 6(b) shows the percentage of eliminated contacts during the compact ejection. This parameter quantifies the stability of the particles, which is related to the final compact's appearance. As one can see, two groups are clearly identified. The results that were obtained in EDEM and using the SJKR2 model in LIGGGHTS indicated a greater compact stability in comparison with the results obtained using the SJKR model. The percentage of eliminated contacts was greater in the latter case. It is also due to the difference between the calculations of the cohesion force, as above mentioned. A little expansion of the disc occurs after the matrix has been removed in all cases as a consequence of the cease of the confinement force. Therefore, the distance between particles increases due to this expansion and some of the particles that were in contact during the confinement stop being in contact after that. The expansion ends when the tensional state becomes stable. At this moment, the contact force between the particles is lower when the SJKR model is used because the cohesion contact force is lower too. This fact makes the overlap between the particles be lower, i.e. the distance between the particles is greater. For that reason, the amount of contacts that are eliminated is higher when the SJKR model is applied. Moreover, no relationship was found between the PSD or timestep used and the percentage of eliminated contacts.

Regarding the effect of the timestep on the computational cost, this decreased as the timestep increased, as shown in Figure 6(c). This is obvious because the number of iterations that it was necessary to calculate for completing a determined simulation was lower when a large timestep is used than when a low value was adopted. Moreover, the slopes of all the curves decreased heavily at a 5–15% Rayleigh timesteps and slightly from 15% on, especially in simulations using EDEM. In addition, the computational cost required by the simulations that were run in EDEM is greater than the computational cost required for their homologue simulations using the two contact models in LIGGGHTS. This can be because the files that save the results in EDEM increase at each data save interval; that is, it is necessary to read and write those files as many times as there are data points. However, in LIGGGHTS, a new result file is created at each data save interval. Moreover, the computational costs required for both packages would be reduced if GPU were utilised.

In view of these results, a timestep equivalent to a 10% Rayleigh timestep is considered the optimum value because the maximum force remained constant until a 15% Rayleigh timestep in all cases, the percentage of eliminated contacts was not related to the timestep and the major diminution of the computational cost took place between the 5% and 10% Rayleigh timesteps. The selection of this timestep matches the range of critical timestep determined by Thakur et al. [23].

3.2. Effect of the conversion tolerance

Preprints (www.preprints.org) | NOT PEER-REVIEWED | Posted: 4 October 2018 doi:10.20944/preprints201810.0081.v1

Peer-reviewed version available at Materials 2018, 11, 2341; doi:10.3390/ma11112341

Figure 7 shows the effect of using different conversion tolerances to export the 3D models to STL files on the maximum force applied by the punch, percentage of eliminated contacts after the matrix has been removed and computational cost.

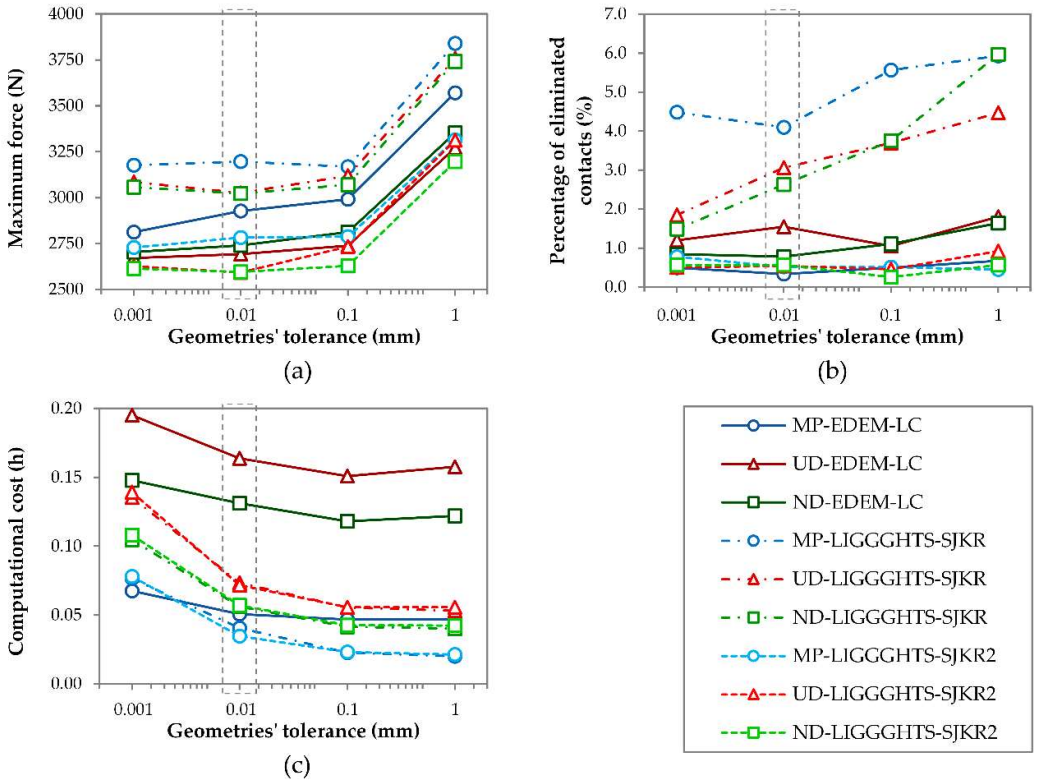

Figure 7. Effect of the conversion tolerance on (a) the maximum force applied by the punch, (b) percentage of eliminated contacts after the matrix has been removed and (c) total computational cost.

The maximum force increased with the conversion tolerance, regardless of the PSD simulated or contact model used, as illustrated in Figure 7(a). This trend arises because the cross-section of the geometries becomes lower as the tolerance increases, as can be seen in Figure 5. The maximum force varied slightly between tolerance values of 0.001 and 0.1 mm, but it increased considerably from 0.1 mm to 1 mm. This is because the prism corresponds to the geometry, where 1 mm of tolerance has only 10 faces. Moreover, one can appreciate that the values of maximum force in the simulations that used the linear cohesion and SJKR2 models were lower than those obtained using the SJKR model, as above shown in Figure 6(a).

Figure 7(b) plots the percentage of eliminated contacts during the compact ejection. As one can see, the results of the simulations run in EDEM and LIGGGHTS using the SJKR2 model were almost unaffected by the conversion tolerance. However, the percentage of eliminated contacts increased strongly with the tolerance when the SJKR model was used. This is probably because the overlaps between particles were greater at the beginning of the ejection process (before the matrix had been removed) as the conversion tolerance was greater because the cross-section was lower and the particles had a smaller volume. This fact happens for all the contact models, but the effect was more marked in the simulations that used the SJKR model because the cohesion force in this model is lower than those calculated for the linear cohesion and SJKR2 models. Thus, the confinement force must be greater for the SJKR model. When this force ceased, the expansion of the disc simulated under the SJKR model was greater than in the other simulations. Moreover, no relationship between the PSD and percentage of eliminated contacts was found.

The difference in the number of faces also affected the computational cost, as illustrated in Figure 7(c). The time simulation decreased as the conversion tolerance increased. This was because the

number of elements that compounded the meshes increased as the mesh size decreased; that is, the number of elements increased as the tolerance decreased. Therefore, the simulation times are higher when the tolerance is lower because the DEM simulators detect the contact between the particles and surfaces (mesh elements). When the mesh size of the geometries is extremely small, the DEM simulators have to check a great number of elements to identify whether the particles contact with them. This was the case for the geometry with 0.001 mm of tolerance, where the simulation time was considerably higher than the time required to simulate the geometry with 0.01 mm. Moreover, the effect of the conversion tolerance on the computational cost was lower in the simulations using EDEM than in their homologues in LIGGGHTS, regardless of the PSD simulated.

In sum, the maximum force increases when the tolerance decreases, percentage of eliminated contacts remains constant (except for the SJKR model) and computational cost decreases with the tolerance, especially from 0.001 mm to 0.01 mm. For these reasons, attending to the effect of the conversion tolerance on the maximum force and computational cost, a tolerance of 0.01 mm was considered optimal.

3.3. Effect of the punch speed

Figure 8 shows the effect of moving the punch at different velocities on the maximum force it applies, percentage of eliminated contacts after the matrix has been removed and computational cost.

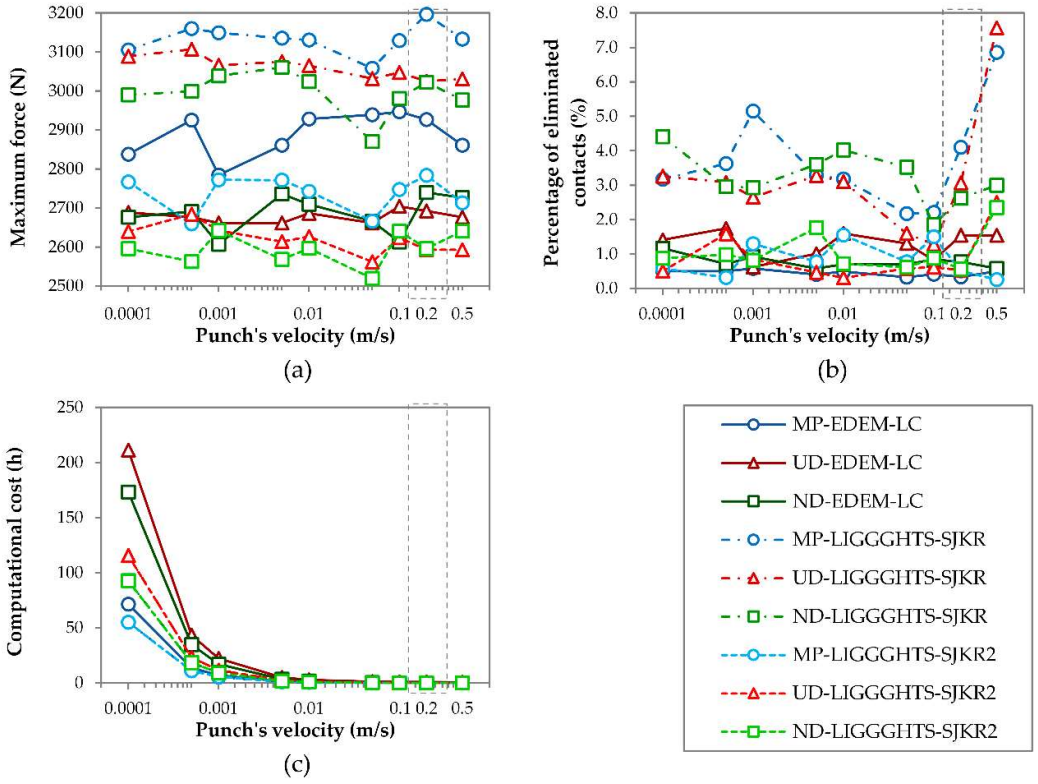

Figure 8. Effect of the speed of the punch on (a) the maximum force applied by the punch, (b) percentage of eliminated contacts after the matrix has been removed and (c) total computational cost.

As one can see in Figure 8(a), the maximum force values fluctuate with the velocities at which the punch moves; thus, it seems that no relationship exists between the speed of the punch and the force it applies. However, it is also possible to appreciate that the results obtained in LIGGGHTS using the SJKR model showed higher values than their homologues using the SJKR2 model or using the linear cohesion model from EDEM did. This is in accordance with the results shown in Figures 6(a) and 7(a). Moreover, the difference between the results obtained using the linear cohesion and SJKR2 models was greater in the case of MP than in the other PSDs.

As Figure 8(b) shows, the percentage of eliminated contacts after the matrix was removed fluctuated with the punch speed up to 0.2 m/s. However, it increased and attained its maximum value at the fastest speed (0.5 m/s) in several cases. In addition, the percentages of eliminated contacts were lower in the simulations that used the linear cohesion and SJKR2 models than in the simulations corresponding to the SJKR model. The amplitude of the fluctuations was also lower in the cases of the linear cohesion and SJKR2 models. However, the curves corresponding to the SJKR model fluctuated greatly. This indicates that the contacts were less stable in the latter case.

The relationship between the computational cost and punch speed is clear: The computational cost increases exponentially as the speed of the punch decreases, as one can see in Figure 8(c), regardless the PSD or contact model used. This is due to the simulation time increase from 0.05 seconds (when the punch moves at 0.5 m/s) to 250 seconds (when the punch's speed is 0.0001 m/s). Therefore, this latter simulation requires 5000 times the number of interactions that the first one requires. In view of these results, a punch speed of 0.2 m/s can be considered the optimal value due to the following factors: (1) there is no relationship between the maximum speed of the punch and the maximum force that it applies; (2) the percentage of eliminated contacts fluctuates with the speed of the punch up to 0.2 m/s, but it increases at 0.5 m/s in some cases; and (3) the computational cost decreases exponentially as the speed of the punch increases.

3.4. Effect of the PSD

In general, PSDs can be sorted according to the values of maximum force in descending order as MP, UD and ND, as illustrated in Figures 6(a), 7(a) and 8(a). This is because the rearrangement of the particles during the confined compression is affected by the PSD, as Wiacek and Molenda [12] indicated. This reorganisation of particles is easier in the cases of UD and ND than in the case of MP because of the presence of large voids filled by the smaller particles. This makes the volume that the particles occupy in MP greater than the volumes that the particles in UD and ND occupy after rearrangement. Therefore, a greater force is necessary to apply to the material MP to compress them into a cylindrical cavity with a diameter of 22 mm and height of 8 mm. Moreover, this behaviour means that the powder relating to the MP distribution is less compressible than the UD and ND powders are. Alternatively, it is not clear that the percentage of eliminated contacts were related to the PSD. Regarding the computational cost, the PSDs can be sorted in ascending order, as follows: MP, ND and UD. This classification is due to the number of particles that were simulated in each case and the minimum particle size they contain. First, the minimum computational costs were required for the MP distribution. This PSD contains 556 particles with a diameter of 2.1 mm. Second, the ND was composed of 698 particles with diameters between 1.2 and 3 mm and demanded intermediate times. Finally, although the UD used the same range of size particles as the ND, the UD needed the maximum computational costs because it used a greater number of particles (922).

3.5. Comparison between the contact models

Figure 9 shows the mean relative difference between the results obtained in LIGGGHTS (using both models) and EDEM. These values are calculated by taking the results obtained in EDEM as a reference, as follows:

$$Mean\ relative\ difference\ (\%) = \frac{\sum_{i=1}^{n}\left(\frac{\left|X_{LIGGGHTS,i}-X_{EDEM,i}\right|}{X_{EDEM,i}}100\right)}{n} \quad (15)$$

where n is the number of simulated setups and $X_{LIGGGHTS,i}$ and $X_{EDEM,i}$ are the results obtained in setup no. i (maximum force or percentage of eliminated contacts) using one of the LIGGGHTS models (SJKR or SJKR2) or EDEM, respectively.

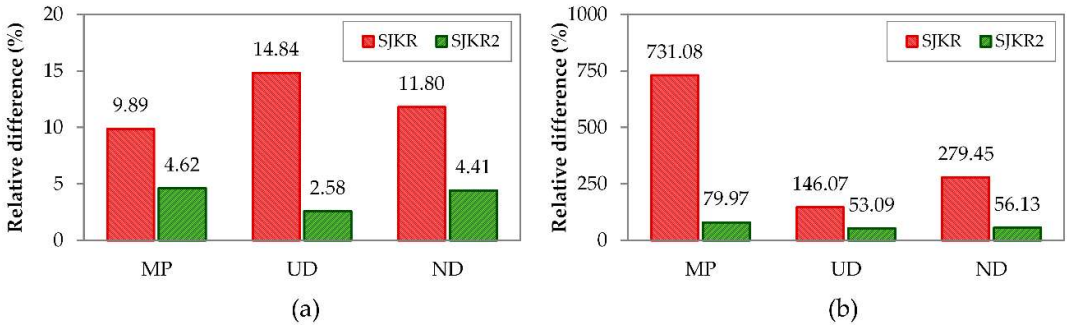

Figure 9. Mean relative difference between the results obtained in LIGGGHTS and EDEM. Difference relating to (a) maximum force and (b) percentage of eliminated contacts.

As visible in Figure 9, the relative difference using the SJKR2 model is lower than that using the SJKR model. This means that the results relating to the maximum force and percentage of eliminated contacts obtained in LIGGGHTS using the SJKR2 model were more similar to the results obtained in EDEM (linear cohesion) than those obtained using the SJKR model. Regarding the maximum force, in Figure 9(a), the relative difference between the linear cohesion and SJKR2 models is lower than 5% in all cases, but it is greater than 9% when the results between linear cohesion and SJKR are compared. The mean relative differences corresponding to the percentage of eliminated contacts can be seen in Figure 9(b). This plot indicates greater relative differences than those shown for the maximum force. Moreover, the difference between the SJKR and linear cohesion models is extensive, especially in the case of MP, where the relative difference is higher than 700%. However, the relative differences between the linear cohesion and SJKR2 models are lower than 80% in all cases.

As mentioned above (see Figures 6, 7 and 8), the maximum forces that were applied by the punch using the SJKR model are greater than those obtained using the SJKR2 and linear cohesion models. The percentages of eliminated contacts were also greater in the case of SJKR. These differences may be because the contact area is calculated in a different way in the latter contact model, as mentioned above. Therefore, the contact force that is proportional to the contact area is different in both cases. This force affects the distance between particles, and consequently, the apparent volume of the material and force applied by the punch. However, this difference has little influence on the computational cost. Regarding this factor, the linear cohesion model is the contact model with the highest computational cost requirements.

4. Conclusions

Several simulations were performed to examine the capability of certain contact models to simulate a compaction process. For this purpose, three contact models were tested. All allowed forming a compact via the particles' cohesion. Nevertheless, some differences were observed between them. This made it possible to obtain the equivalent DEM models implemented in two different simulators (EDEM and LIGGGHTS). In addition, different values of timestep, conversion tolerance and punch speed were used. Moreover, three PSDs were simulated to investigate the influence of these parameters on the results obtained using each PSD. Thus, the following conclusions were established:

- Regarding the timestep, its selection determines the maximum force that the punch applies due to the inaccuracy of the calculus when a long timestep is chosen. The results showed that the maximum force is lower when the timestep is higher. Moreover, the computational cost decreases with the increment of this simulation parameter. However, the percentage of eliminated contacts does not depend on the selected timestep. Finally, a value of 10% of Rayleigh time was adequate for simulating the compaction process using the contact models employed in this work;

- Concerning the conversion tolerance, the force applied by the punch increases as the tolerance of the geometries increases because the cross-section is lower when the tolerance is higher. The behaviour of the percentage of eliminated contacts differs depending on the applied contact model. The conversion tolerance does not influence the percentage of eliminated contacts when the linear cohesion or SJKR2 model is used. However, the percentage of eliminated contacts increases as the tolerance rises when the SJKR model is selected. Contrary to the maximum force, the computation cost decreases as the conversion tolerance increases because the number of faces is lower in those geometries where the tolerance is higher. For these reasons, the tolerance that is recommended for converting the 3D models to STL files is equal to 0.01 mm for the geometries used in this work;
- Regarding the punch speed, the maximum force fluctuates with this parameter. Therefore, no relationship between the two was found. The percentage of eliminated contacts also fluctuated, but the maximum values were attained at a speed of 0.5 m/s for several cases. However, the computational cost is strongly influenced by the punch speed. Consequently, the maximum speed at which it is recommended to move the punch is 0.2 m/s; and
- Concerning the PSD of the materials, the maximum forces were obtained for the MP distribution because the particle rearrangement is more difficult in this context than it is in other PSDs. However, no relationship between the percentage of eliminated contacts and PSD was found. The lowest computational costs were required for the MP distribution because a small number of large particles were created in those simulations. However, a greater number of small particles composed the other PSDs. Moreover, the simulations that used the UD distribution required the greatest computational costs because they used the greatest number of particles.

Finally, the conclusions relating to the contact models and software packages are as follows: Although the results obtained using the three contact models were similar, a greater difference was found in the results relating to the SJKR model. Therefore, the linear cohesion model implemented in EDEM and SJKR2 model in LIGGGHTS can be considered equivalent contact models.

This work is focused on the analysis of the differences and similarities between several contact models, but it is supposed to be a starting point to study the compaction process. In future works, the optimal values that were determined in this study will be fixed, and the influence of other parameters will be examined. Moreover, the applicability of the equivalent contact models for simulating the compaction of real materials will be analysed. This will make it possible to understand the process and find solutions to the problems that usually occur during the formation of green compacts.

Author Contributions: J. O-M. proposed the research topic ; C. R-A. performed the DEM simulations, analysed the results and wrote the manuscript; F. A-E. and A. G-M. guided and supervised the project. All the authors revised the manuscript and contributed some useful suggestions in pre-publication stage.

Funding: This work was funded by the EU programme RFSR through project RFSR-CT-2015-00005 'LEANSTORY'.

Acknowledgments: The discrete element method (DEM) simulations and analysis were conducted using EDEM® 2.7.2 bulk material simulation software that was provided by DEM Solutions Ltd., Edinburgh, Scotland, UK and LIGGGHTS-PUBLIC 3.3.1 open-source. The authors want to acknowledge the contribution provided by the Materials Engineering degree thesis carried out by Mr Luis Domingo Aranda, although specific citation was added when appropriate.

Conflicts of Interest: The authors declare no conflict of interest.

References

1. Gupta, N.; Basu, B. Hot pressing and spark plasma sintering techniques of intermetallic matrix composites. In *Intermetallic Matrix Composites*; Rahul Mitra, Ed.; Elsevier Woodhead Publishing, 2018; pp. 243–302 ISBN 9780857093462.
2. Suk-Joong L. Kang *Sintering. Densification, Grain Growth, and Microstructure*; 1st ed.; Elsevier Butterworth-

Heinemann, 2005; ISBN 978-0-7506-6385-4.

3. Furlani, E.; Aneggi, E.; Maschio, S. Sintering behaviour of waste olivine and olivine/alumina blends. *Materials* **2014**, *7*, doi:10.3390/ma7064773.
4. Naglieri, V.; Palmero, P.; Montanaro, L.; Chevalier, J. Elaboration of alumina-zirconia composites: Role of the zirconia content on the microstructure and mechanical properties. *Materials* **2013**, *6*, 2090–2102, doi:10.3390/ma6052090.
5. Ye, X.; Li, Y.; Ai, Y.; Nie, Y. Novel powder packing theory with bimodal particle size distribution-application in superalloy. *Adv. Powder Technol.* **2018**, *29*, 2280–2287, doi:10.1016/j.apt.2018.06.012.
6. Arifvianto, B.; Zhou, J. Fabrication of metallic biomedical scaffolds with the space holder method: A review. *Materials* **2014**, *7*, 3622, doi:10.3390/ma7053588.
7. Miyake, K.; Hirata, Y.; Shimonosono, T.; Sameshima, S. The Effect of Particle Shape on Sintering Behavior and Compressive Strength of Porous Alumina. *Materials.* **2018**, *11*, doi:10.3390/ma11071137.
8. Janda, A.; Ooi, J. Y. DEM modeling of cone penetration and unconfined compression in cohesive solids. *Powder Technol.* **2016**, doi:10.1016/j.powtec.2015.05.034.
9. Thakur, S. C.; Ahmadian, H.; Sun, J.; Ooi, J. Y. An experimental and numerical study of packing, compression, and caking behaviour of detergent powders. *Particuology* **2014**, doi:10.1016/j.partic.2013.06.009.
10. Aranda-Sánchez, L. D. Simulación numérica de las propiedades del refractario libre de carbono, Polythecnic University of Madrid: Madrid, Spain, 2016.
11. Nordström, J.; Alderborn, G.; Frenning, G. Compressibility and tablet forming ability of bimodal granule mixtures: Experiments and DEM simulations. *Int. J. Pharm.* **2018**, doi:10.1016/j.ijpharm.2018.02.006.
12. Wiącek, J.; Molenda, M. Effect of particle size distribution on micro-and macromechanical response of granular packings under compression. *Int. J. Solids Struct.* **2014**, doi:10.1016/j.ijsolstr.2014.06.029.
13. Wiacek, J.; Molenda, M.; Horabik, J.; Ooi, J. Y. Influence of grain shape and intergranular friction on material behavior in uniaxial compression: Experimental and DEM modeling. *Powder Technol.* **2012**, doi:10.1016/j.powtec.2011.10.060.
14. He, Y.; Evans, T. J.; Shen, Y. S.; Yu, A. B.; Yang, R. Y. Discrete modelling of the compaction of non-spherical particles using a multi-sphere approach. *Miner. Eng.* **2018**, doi:10.1016/j.mineng.2017.12.013.
15. Jiménez-Herrera, N.; Barrios, G. K. P.; Tavares, L. M. Comparison of breakage models in DEM in simulating impact on particle beds. *Adv. Powder Technol.* **2018**, *29*, 692–706, doi:10.1016/j.apt.2017.12.006.
16. Wei, H.; Zhao, Y.; Zhang, J.; Saxén, H.; Yu, Y. LIGGGHTS and EDEM application on charging system of ironmaking blast furnace. *Adv. Powder Technol.* **2017**, doi:10.1016/j.apt.2017.05.012.
17. Markauskas, D.; Ramírez-Gómez, Á.; Kacianauskas, R.; Zdancevicius, E. Maize grain shape approaches for DEM modelling. *Comput. Electron. Agric.* **2015**, *118*, 247–258, doi:10.1016/j.compag.2015.09.004.
18. Soltanbeigi, B.; Podlozhnyuk, A.; Papanicolopulos, S. A.; Kloss, C.; Pirker, S.; Ooi, J. Y. DEM study of mechanical characteristics of multi-spherical and superquadric particles at micro and macro scales. *Powder Technol.* **2018**, doi:10.1016/j.powtec.2018.01.082.
19. Kozhar, S.; Dosta, M.; Antonyuk, S.; Heinrich, S.; Bröckel, U. DEM simulations of amorphous irregular shaped micrometer-sized titania agglomerates at compression. *Adv. Powder Technol.* **2015**, *26*, 767–777, doi:10.1016/j.apt.2015.05.005.
20. Cundall, P. A.; Strack, O. D. L. A discrete numerical model for granular assemblies. *Géotechnique* **1979**, *29*, 47–65.
21. DEM Solutions. EDEM 2.6 Theory reference guide 2014.
22. Wang, H.; Glaser, B.; Sichen, D. Improvement of Resistance of MgO-Based Refractory to Slag Penetration

by In Situ Spinel Formation. *Metall. Mater. Trans. B Process Metall. Mater. Process. Sci.* **2015**, *46*, 749–757, doi:10.1007/s11663-014-0277-7.

23. Thakur, S. C.; Ooi, J. Y.; Ahmadian, H. Scaling of discrete element model parameters for cohesionless and cohesive solid. *Powder Technol.* **2016**, doi:10.1016/j.powtec.2015.05.051.